New Actuator Disk Model for the Analysis of Wind Turbines Wake Interaction with the Ground

S. Adjiri[1,3†], I. Dobrev[2], A. Benzaoui[3], H. Nedjari-Daaou[1] and F. Massouh[2]

[1] EPST Centre De Développement Des Enregies Renouvelables, CDER, BP 62 Route de l'Observatoire,
Bouzareah, 16340, Alger, Algeria
[2] DynFluid, ENSAM, 151 bvd L'Hopital; 75013 Paris France
[3] Thermodynamics and Energetical Systems Laboratory, Faculty of Physics, USTHB, B.P 32 El Alia, 16111
Bab Ezzouar-Algiers, Algeria

†Corresponding Author Email: s.adjiri@cder.dz

ABSTRACT

Wake models based on Actuator Disk theory are usually applied to optimize the wind farm layouts and improve their overall efficiency and expected AEP. Despite the effectiveness of the existing models, most Actuator Disk approaches are based on the flow axisymmetric assumption, without considering the ground effect on the wake behavior. However, it has been shown that the mast's height, or distance from the wind turbine to the ground, has an influence on the wake expansion on both hub's side and at downstream of the wind turbine. Therefore, in this study, a hybrid CFD-BEM-Actuator Disk approach is developed to address the lack of the existing models. In the proposed model, the 3D wind rotor is modeled by a set of blade elements. Then, the local lift and drag forces acting on each blade element are calculated using BEM theory and incorporated into the momentum equation. This BEM-AD model is implemented in a User Defined Function (UDF) that is loaded into the CFD software. Thereby, ground effects are considered to be a wall boundary and defining a wind boundary layer profile at the inlet boundary, which describes the Atmospheric Boundary Layer (ABL). For the validation of this new Actuator Disk model, an enhanced experimental study is conducted at the Dynfluid Laboratory wind tunnel (ENSAM School Paris Tech). The Particle Image Velocimetry (PIV) measurements are used for the experimental wake explorations applied to a miniature two-bladed wind turbine. The wake developments are analyzed at two different hub heights ratio, $h/D = 0.7$ and 1.0 (where h is the hub height, and D is the wind rotor diameter). The analysis of the outcomes showed that the numerical simulations are in good correlation with the experimental measurements of the ENSAM wind tunnel. The numerical results show that for $h/D=0.7$, the upper half of the rotor operates within the boundary layer whereas the lower tip vortices are mainly developed in the horizontal direction with lower intensity compared to the upper tip vortices. This effect was not observed for the case $h/D=1.0$ where the rotor operates outside of the boundary layer; however, the wake centerline is upward deflected at about 0.3D. The main conclusion is that a distance above 7D must be observed between wind turbines to optimize the wind farm performance and over 1D hub height be required to limit the influence of the ground boundary layer effect.

Keywords: Wind turbine wake; BEM-Actuator Disk model; CFD, Wall-model; Wind tunnel.

NOMENCLATURE

AEP	Annual Energy Production	P	atmospheric pressure
a	thickness of the airfoil blade	p	pressure coefficient
Cx	force coefficient in x direction	r	rotor radius
Cy	force coefficient in y direction	r_c	diameter of the nacelle
$C_{\varepsilon 1}$	turbulence model constant	T	rotor rotation period
$C_{\varepsilon 2}$	turbulence model constant	th	thickness of the rotor disk
Cd	drag coefficient	U_0	inlet velocity
Cl	lift coefficient	U(z)	axial velocity
$C_{d, nac}$	Nacelle drag coefficient	u^*_{ref}	friction velocity at H_0.
Cμ	turbulence model constant	u_i	velocity component
C_R	constant	x_i	Cartesian coordinates
C_s	constant	*x*	lateral component

c	chord	y	transversal component
D	rotor diameter	y_0	ground roughness length
d	hub diameter	y_p	mesh height of the first cell
dt	time step	z	axial component
F_x	X component of pressure force		
F_m	volumetric force		
$F_{L,D}$	force applied on a blade element δr	***Greek letters***	
f, g	generic functions	α	angle of attack
fp	calibrate scalar function	$\delta\theta$	azimuthal element
$f_{body,i}$	volume forces induced by the rotor	δr	radial element
H_0	reference height	ε	dissipation rate
h	hub height	λ	tip speed ratio
i	time index	ρ	air density
j	space index	θ	azimuthal position
K	turbulent kinetic energy	υ_t	turbulent viscosity
κ	Von Karman constant	υ	viscosity
Ly	domain dimension in lateral direction	σ_k	constant in the turbulent kinetic energy model
Lx	domain dimension in transversal direction	σ_s	constant in the turbulence dissipation model
Lz	domain dimension in axial direction	ϵ	absolute relative error
N	number of blades.	ω	angular velocity
P_k	turbulence energy production	ω_z	axial vorticity

1. INTRODUCTION

The world new development imposes the end of fossil energy sources. To deal with the energy and environmental crisis, the use of renewable energies seems to be the best alternative. Indeed, thanks to the impressive development achieved in recent years, wind power can produce tens of MWh per site. Wind farm experiences around the world have emerged and succeeded in meeting their objectives (Wind energy in Europe Report 2019). However, the challenge in large-scale wind farms remains the wind turbines layout optimization in order to reduce the wake effects generated by the wind rotors and thereby reduce energy losses and reduce the risk of fatigue, which may be due to high aerodynamic loads (Breton 2008).

Several numerical and experimental studies have been performed for the analysis and exploration of the detailed wake structures affecting the wind farm performance (García Regodeseves and SantolariaMorros 2021). In recent years, full rotor models based on Computational Fluid Dynamics (CFD) methods have been widely used (Makridis and Chick 2013; Javaherchi *et al.* 2014; Daaou Nedjari *et al.* 2020). However, significant computer resources allowing the simulation of a complete geometry of wind turbines are required. Thus, to reduce the cost and the CPU time, hybrid models consisting in modeling the rotor by an actuator disk have been developed. In these approaches, the aerodynamic forces are introduced as source terms in the momentum equations. In several works using the actuator disk model the aerodynamic forces are expressed in the axial direction only, and consider a uniform load distribution along the rotor blade (Sørensen and Myken 1992; Ammara *et al.* 2002; Masson 2006; Stevens *et al.* 2017).

In order to enhance the axis symmetric wake models performance, (El Kasmi and Masson 2008) developed an improved Actuator Disk model by introducing a reduction of the dissipative effect in the wind turbine wake and adding an additional dissipative term for turbulence. They significantly enhanced the wake intensity evolution downstream of the Nibe 630kW and the Danwin 180kW wind turbines.

These assumptions ignore the effects of the tangential and normal forces applied in the two other directions that cause a decrease in wake expansion. Therefore, the accuracy of the information on the wake size downstream of the rotor is reduced and consequently influences the optimization of the wind farm layout.

An additional constraint for these wake models is the hypothesis which considers a perfect flow symmetry on either side of the rotor, and ignores the effect of the ground on the wake expansion.

The ground effect on wake expansion has been addressed in the study of wind rotor interactions with the Earth boundary layer, which is extremely important given the turbulence, the unsteadiness of the flow as well as the thermal and diurnal effects encountered (El-Askary and Sark 2017). It is thus essential to know the ABL structure and the changes that occurred in it.

Modeling wind wake turbulence has received a lot of interest in recent years where the choice of the turbulence model can be predicted by the interval of the turbulence spectrum. Direct Numerical Simulation (DNS) is cumbersome and expensive as it resolves all length scales (Ducoin *et al.* 2017). Two author turbulence-modeling techniques are widely applied for the study of the large-scale wind turbine wake: the Reynolds-Averaged Navier Stokes (RANS) models and the Large Eddy Simulation (LES) model. The RANS model use the concept of turbulent viscosity, which provide a valuable saving in computation time (Hussein and El-Shishiny 2012) and the LES model is based on the separation of large and small scale eddies (Wu and Porté-Agel 2011;

Stevens *et al.* 2017; Boojari *et al.* 2019). Gao *et al.* (2021a) combined the Actuator line method with LES computations to compute the near and far wake regions of wind turbines. Johlas *et al.* (2022) used the SOWFA LES tool developed by the National Renewable Energy Laboratory (*NREL*) to investigate the turbine wake with tilted rotor, where the wind turbine rotor has been modeled by the actuator disk model. Although the numerical accuracy of the LES methods applied to the simulation of wind turbine wakes and considering their computational cost, the RANS methods are still in use and remain efficient particularly for the simulation of a standalone wind turbine wakes as noticed by Gao *et al.* (2021a).

Furthermore, numerical and experimental works have shown that the wake is distinguished by two regions, the near and the far wake (Vermeer 2003; Gunn 2019). The near wake zone is characterized by vortices generated at the base and the tip of blade, with different intensities, thus creating a sheet of marginal vortices of helicoidal trajectory. The far wake zone is characterized by an attenuation of the previous vortex structure, which gives way to the wake interaction with more turbulent atmospheric flow in this zone (Simisiroglou1 *et al.* 2016).

Moreover, it has been noted that both near and far wakes are also disturbed by the distance to the ground (the hub height effect) that increases the downstream turbulence state (Abkar and Porté agel 2014). These disturbances lead to unstable operations of adjacent wind rotors. (Daaou Nedjari *et al.* 2017) showed that the ground proximity can increase turbulence in the near wake and affect the wake shape and symmetry. (Porté agel *et al.* 2020) described the effect of hub-induced vortex that are animated by a periodic motion observed in the near wake. Thereby, the ground proximity effect can have a significant influence on the wake downstream, which can increase turbulence and create a delay in wake development.

On the other hand, important experimental studies were conducted, whether in a wind tunnel or in free atmosphere under real conditions. (Aubrun *et al.* 2013) explored the wake properties of a porous disk model and a small wind turbine in two different atmospheric conditions. (Chamorro *et al.* 2012) conducted experiments on the wind turbine wake in a wind tunnel by introducing a heat flow to model the instable atmospheric conditions. In recent studies carried out in wind tunnel on scale models of wind turbines, high-precision flow exploration methods are used. The non-intrusive method of Particle Image Velocimetry (PIV) is one of the most effective methods used (Massouh and Dobrev 2007; Kamada and Maeda 2011; Espanâ *et al.* 2012; Dobrev *et al.* 2013; Abdulrahim *et al.* 2016).

Large-scale experimental work by (Hong 2014) showed the vortex structures of the wake flow behind a single 2.5 MW wind turbine and observed blade tip vortices from snow particles motion under real atmospheric conditions. The structure and evolution of the tip vortices have been highlighted by identifying their imprints on the atmospheric flow

with the formation of vacuum zones above the vortices.

As shown, the wake consists of a complex vortex generated by the blade interaction with the ABL turbulence structures.

The disturbance effect on the ABL due to the wake, produces a significant impact on the energy losses in a wind farm, which induces an economic impact and makes wake studies relevant and still up-to-date. This work proposes numerical and experimental investigations of the wake-ground interaction within the neutral atmospheric boundary layer. The numerical study consists on the development of a hybrid Actuator-BEM model, based on the blade element momentum theory coupled with computational fluid dynamics (CFD). The hybrid model is proposed to save computation time and cost, while taking into account the influence of the ground and the non-uniform loading of the rotor. To consider the blade rotation effects, the axial, normal and tangential aerodynamic forces are determined as function of the blade geometry and airfoil data. These forces are expressed as a source term in the momentum equations. The wind tunnel study is carried out under controlled conditions where the PIV method is used to explore the structure of the two bladed wind turbine wake.

This study is applied to a two-bladed wind turbine. The near and far wake as well as its interaction with the ground are investigated. The velocity deficit is calculated downstream the rotor at the axial distance to diameter ratios z/D varying from 1 to 7. The effect of the hub height on the wake development is investigated for two height to diameter ratios, h/D = 0.7 and h/D = 1.

2. GOVERNING EQUATIONS

The unsteady Navier Stokes equations are solved in a 3-D computational domain. The rotating forces acting on the wind rotor are included in the momentum equations as source terms.

$$\frac{\partial \mathbf{u}_i}{\partial x_i} = 0 \tag{1}$$

$$\frac{\partial \mathbf{u}_i}{\partial t} + u_j \frac{\partial \mathbf{u}_i}{\partial x_j} = -\frac{1}{\rho} \frac{\partial p}{\partial x_i} + \frac{\partial}{\partial x_j} \left[\left(\nu + \nu_t \right) \left(\frac{\partial \mathbf{u}_i}{\partial x_j} + \frac{\partial \mathbf{u}_j}{\partial x_i} \right) \right] + f_{body,i} \tag{2}$$

Where ρ is the air density, p the atmospheric pressure, u_i, u_j are the components of the velocity field and x_i, x_j are the Cartesian coordinates. $f_{body,I}$ represents the volume forces induced by the rotor that are computed by the BEM-AD method described in section 4.

2.1 Turbulence Modeling

The turbulence model used is the modified k-ε model. The additional turbulent viscosity brought by the Bousinesq formula is expressed by:

$$\nu_t = C_\nu \frac{k^2}{\varepsilon} \tag{3}$$

with

$$\varepsilon = v \frac{\partial \overline{u_i}}{\partial x_j} \frac{\partial \overline{u_j}}{\partial x_i} \tag{4}$$

Two transport equations binding to the turbulent kinetic energy k and the dissipation rate ε are therefore added to equations (1) and (2) as follows

$$\frac{\partial k}{\partial t} + U_i \frac{\partial k}{\partial x_i} = \frac{\partial}{\partial x_i}\left(\left(v + \frac{v_t}{\sigma_k}\right)\frac{\partial k}{\partial x_i}\right) + p_k - \varepsilon \tag{5}$$

$$\frac{\partial \varepsilon}{\partial t} + U_i \frac{\partial \varepsilon}{\partial x_i} = \frac{\partial}{\partial x_i}\left(\left(v + \frac{v_t}{\sigma_k}\right)\frac{\partial \varepsilon}{\partial x_i}\right) + C_{\varepsilon 1}\, p_k \frac{\varepsilon}{k} - C_{\varepsilon 2}\frac{\varepsilon^2}{k} \tag{6}$$

Where p_k is the turbulent energy production, indicating the interaction between turbulence fluctuations and mean flow, it is expressed as follows:

$$P_k = v_t \frac{\partial u_i}{\partial x_j}\left(\frac{\partial u_i}{\partial x_j} + \frac{\partial u_j}{\partial x_i}\right) \tag{7}$$

Where C_v, $C_{\varepsilon 1}$, $C_{\varepsilon 2}$, σ_k and σ_ε are the k-ε model constants. The standard constants have been modified to be closer to atmospheric conditions and the values proposed by (Panofsky and Dutton 1984) are used. The applied model constants are thus:

C_v=0.033, $C_{\varepsilon 1}$ = 0.176, $C_{\varepsilon 2}$=1.92, σ_k=1 and σ_ε=1.3

3. THE ABL WIND PROFILE

The ABL flow is set by the logarithmic velocity profile proposed by (Panofsky 1988; Tominaga *et al.* 2008) and written as follows:

$$V(H) = \frac{u_{ref}^*}{K}\ln\left(\frac{H + H_0}{H}\right) \tag{8}$$

with

$$u_{ref}^* = \frac{\kappa U_{ref}}{\ln\left(\frac{H_{ref} + H_0}{H_{ref}}\right)} \tag{9}$$

Where κ=0.4187 is the Von Karman constant.

The inlet turbulent kinetic energy K and dissipation rate ε are defined as in (Blocken *et al.* 2007; Shen *et al.* 2009) and expressed as follow:

$$k = \frac{u_{ref}^2}{\sqrt{C_\mu}} \tag{10}$$

$$\varepsilon(H) = \frac{u_{ref}^3}{K(H + H_0)} \tag{11}$$

The atmospheric boundary layer settings are loaded into the CFD code as UDF. Cμ= 0.033 is the modified constant for neutral air boundary layer flows based on (Panofsky and Dutton 1984).

4. HYBRID BEM-ACTUATOR DISK MODEL

A BEM-Actuator Disk hybrid model (BEM-AD) is applied to explore the development of the near and far wind turbine wake. The interaction of the wake with the ground is investigated to evaluate the hub height effects on the wake expansion.

The aerodynamic forces, introduced in the Navier-Stokes equations as source term, are distributed on each volume element as shown in Fig. 1. The local axial and tangential forces are computed according to the blade geometry and the aerodynamic profile data. The forces are calculated using the velocity field computed by the CFD solver at each time step.

In the BEM-AD model, the rotor disk is divided into sectors with an azimuthal angle δθ and a radius R, each sector consisting of elements of length δr. The volume forces, $\delta F_{m\,L,D}$, are computed on each blade element δθ x δr as follows:

$$\delta F_{m\,L,D} = \delta F_{L,D}\frac{\delta t}{T} = \delta F_{L,D}\frac{N\delta\theta}{2\pi} \tag{12}$$

Where $\delta F_{L,D}$ are the forces on the blade element computed at each time step δt= δθ/ ω, and T is the rotation period defined as:

$$T = \frac{2\pi}{N.\omega} \tag{13}$$

ω is the angular velocity of the rotor disk and N is the number of blades.

The forces $\delta F_{L,D}$ obtained by the blade element theory are calculated using the following formula:

$$\delta F_{L,D} = \rho\frac{W^2}{2}C_{L,D}(\alpha)c(r)\delta r \tag{14}$$

Where $C_{L,\,D}$ are the blade section lift and drag coefficients as shown in Fig. 2, and α is the local angle of attack.

The average force of the blade applied to the actuator surface element is computed by substituting Eq. (12) in Eq. (14)

$$\delta F_{m\,L,D} = \rho\frac{W^2}{2}C_{L,D}(\alpha)c(r)\delta r\frac{N\delta\theta}{2\pi} \tag{15}$$

For an actuator disk of thickness th, the volume of the annular element is dV = δr * rδθ * h. The force per unit volume are thus:

$$f_{L,D} = \frac{\delta F_{m\,L,D}}{\delta V} = \rho\frac{W^2}{2}C_{L,D}(\alpha)c(r)\frac{N}{2\pi rth} \tag{16}$$

The W formulation is as follow:

$$W = \sqrt{(\omega r + u_i)^2 + V^2} \tag{17}$$

The axial velocity V and the tangential velocity u_i are obtained from the CFD calculations.

The lift and drag forces are projected on the axial and tangential directions (Fig. 2):

$$\delta f_a = \delta f_L \cos(\alpha) + \delta f_D \sin(\alpha) \tag{18}$$
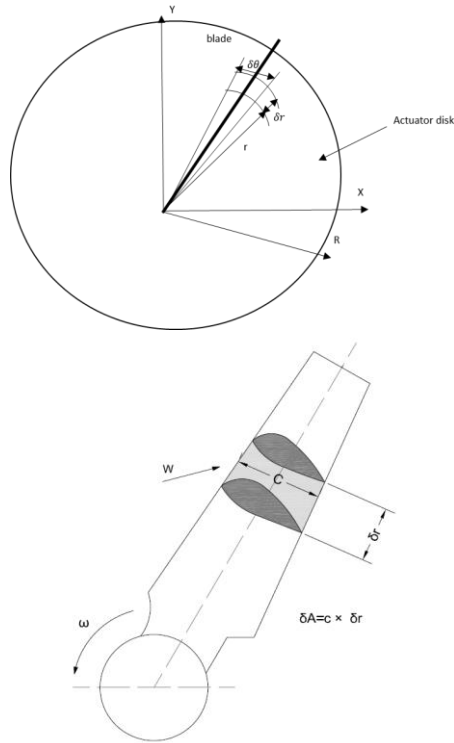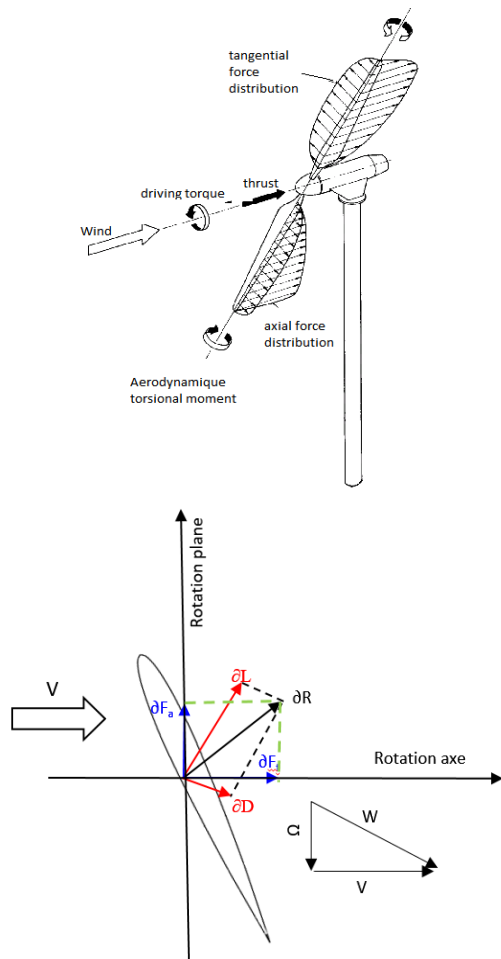
Fig. 1. BEM-Actuator Disk concept.

Fig. 2. Aerodynamic forces projection on the twin-blade wind turbine profile.

$$\delta\!f_t = \delta\!f_L \sin(\alpha) + \delta\!f_D \cos(\alpha) \tag{19}$$

The axial and tangential forces are expressed in Cartesian coordinates and added as source terms in the momentum equations to consider the effects of the turbine rotor on the flow:

$$\begin{cases} f_x = -f_t \sin\theta \\ f_y = f_t \cos\theta \\ f_z = f_a \end{cases} \tag{20}$$

4.1 Tip Loss Correction

To include three-dimensional tip loss effects, (Shen *et al.* 2005) introduced a correction factor F1 to the 2D airfoil lift and drag coefficients as follows:

$$C_{L,D} = F_1 C_{L,D}^{2d} \tag{21}$$

With

$$F_1 = \frac{2}{\pi} \cos^{-1}\left[\exp\left(-g\, \frac{N(R-r)}{2r\sin\alpha} \right) \right] \tag{22}$$

Where R is the turbine radius and g is a depending function expressed as:

$$g = \exp\left[-0.125(RN\omega/V_\infty - 21) \right] + 0.1 \tag{23}$$

4.2. Nacelle Modeling

As has been shown in many articles, the nacelle has a significant influence on the propagation of the wind turbines wake. To consider this effect, different approaches have been applied for the modeling of the nacelle. Gao *et al.* (2021b) carried LES computations coupled with an actuator line method to investigate the wind turbine wake. To improve the numerical accuracy of the near-wake results, they included the modeling of the tower and nacelle by body forces projected into the flow field using a piecewise function. In De Cillis *et al.* (2022) work, the tower and nacelle were described by the immersed boundary method (IBM). This method consists in imposing the velocity inside the body equal to zero. At the first point adjacent to the body, the Navier–Stokes equations are not discretized, and the velocities are evaluated by linear interpolation from those at the second external point (Orlandi and Leonardi 2006). In this study, as the applied BEM-AD method consists in adding source terms in the momentum equations for the rotor modeling, the nacelle is also modeled by source terms added to the momentum equations and solved for the nacelle volume. The nacelle of the considered wind turbine is a circular cylinder with diameter of $r_c=2.5$mm, therefore a constant drag coefficient $C_{d,\,nac} = 1.2$ is applied. This approach allows to consider the influence of the nacelle on the wake downstream of the rotor while reducing the computation time.

5. EXPERIMENTAL SETUP

The wake experimental study was performed in the Dynfluid laboratory wind tunnel in a closed loop

with a 3m diameter axial fan. A 120 kW power motor is installed to drive the fan. The test section is preceded by a plenum chamber and a convergent with a large contraction ratio, equal to 12.5, producing a uniform velocity profile up to 40 m/s, with low turbulence. The test section dimensions are respectively: 1.35 m height, 1.65 m width, and 2 m length. The PIV measurements are activated from a signal transmitted by the data acquisition system through a sensor that tracks a reflective target attached to the rotor (Fig. 4).

D=100 mm represents the rotor prototype's diameter with a hub diameter of about d=14 mm. The blade airfoil is a flat plate of a =0.5 mm thickness with a root and tip chord of 9 mm and 6mm respectively. The blades are non-twisted, straight with a pitch angle of 8°.

Two hub heights were tested, h/D =0.7 and h/D =1. The upstream flow velocity is a natural progression of the flow. Due to the ground proximity, the measured velocity profile is parabolic. However, at the wind turbine height, the inlet velocity has a constant value. These experiments are carried out for $U\infty$ = 13.7 m/s with a constant turbine rotational speed Ω =11.900 rpm. The tip speed ratio is thus $\lambda=\omega R/U\infty$ = 4.75. The Reynolds number calculated by mean of tip-chord of the blade and the tip-peripheral velocity U is Re=23000.

The PIV system is monitored by Dantec's Dynamics -Studio 2.30. The images are taken with a Nd-YagLitron Nano-L 200-15, with a power impulse of 200 mJ and two Dantec-Flow-Sense 4M cameras with a resolution of 2048x2048 pixels. The cameras are equipped with lenses Nikkor AF-D 180 mm f/2.8IF ED, for near wake measurements. For far wake measurements, the cameras are equipped with lenses AF Micro-Nikkor 60mm f/2.8D. The acquisition system is equipped with two NI-1428 frame-grabber cards and synchronizes the images with laser flashes. The flow is seeded with micro-droplets of olive oil generated by a mist generator (Dantec 10F03). The average droplet diameter is 2-5 μm. The two PIV cameras, that are synchronized with the azimuthal position of the rotor and operate in parallel, capture the flow field up to a distance of 7D behind the wind turbine (Dobrev 2009).

The near wake is analyzed on several azimuthal planes (from 0° to 165°). Each measurement plan corresponds to 500 shots. Measurements of the far wake are carried out on 6 azimuth planes (0° to 150°), and each measurement plan corresponds to 2x500 shots. The 0° angle is the vertical position of the blades. Due to the laser power limitation and the camera resolution, the velocity field is divided into six overlapping windows. These windows designated as h1, h2, h3, m1, m2 and m3 are presented in Fig. 3.

For all measurements, image capture is synchronized with the rotor and the PIV system is triggered when the blade is positioned at the desired angular position namely when the reference blade is horizontal.
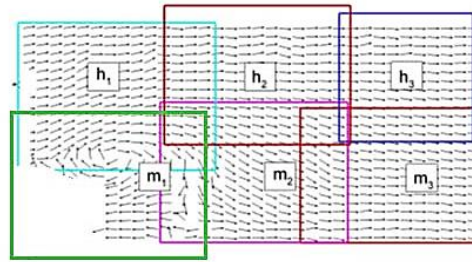

Fig. 3. Planes of the particle positions in the flow.

Fig. 4. Experimental set-up.

6. NUMERICAL MODEL

These unsteady 3D flow computations are performed using the Ansys Fluent 19 CFD software.

6.1 Computational Domain

The domain is composed of a fluid zone and a thin disk which represents the rotor (Figs. 5 and 6). The computational domain is rectangular and has a length L_z =23D, a width L_x = 6.4D and a height L_y = 5D. The disk diameter is D = 100 mm that corresponds to the rotor diameter in the wind-tunnel. The disk thickness is equal to h=0.4D. The Cartesian coordinates origin is set at the rotor center, and the inlet flow is directed along the (z) axis.
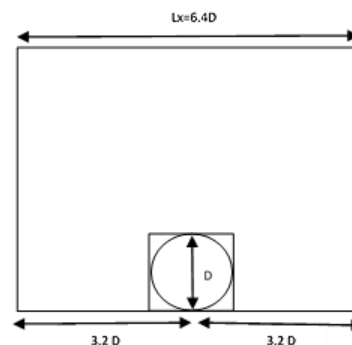

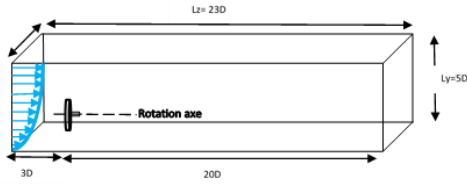**Fig. 5. Computational domain dimensions in the *(xy)* plane.**

Fig. 6. Computational domain.

6.2 Grid Domain

The computational grid contains about 3 to 4 million cells with a fine mesh around the rotor disk and the bottom wall. In the rest of the domain a coarser grid is generated (Fig. 7). The surface of the ground being characterized by a roughness length y_0, the height of the first row of cells above the ground (y_p) should be greater than y_0 (Daaou Nedjari *et al* 2017, Makridis and Chick 2013). We therefore ensure that the condition $y_p > k_s$ is fulfilled, k_s being defined as

$$k_s = \frac{9,793\, y_0}{C_s} \qquad (24)$$

where $C_s \approx 0.5$ is an empirical value introduced by (Réthoré *et al.* 2014).
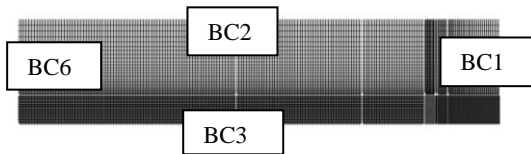
a) Inlet, outlet, top and bottom boundaries.
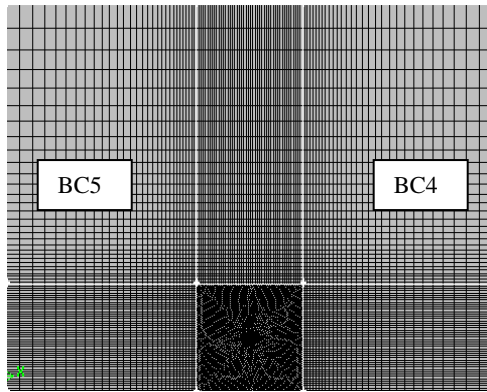
a) Left and right boundaries.

Fig. 7. Computational grid and boundary conditions.

6.3 Boundary Conditions

The boundary conditions used are consistent with the geometry of the wind tunnel test (Fig. 7).

The inlet boundary (BC1) is characterized by the wind boundary layer profile defined in section 3. This profile is implemented in a User Defined Function (UDF). At the top boundary (BC2), a "symmetry" condition is defined, which implies that the velocity vector is parallel to the z-directed flow. At the low boundary of the domain (BC3), wall condition is defined. On the left (BC4) and the right (BC5) boundaries, a "symmetry" condition is imposed, while the "pressure outlet" condition is set at the outlet boundary (BC6). This study is applied to a wind turbine located in a wind tunnel with flat ground, without relief. As flat terrains are characterized by roughness length that varies from 3.10^{-3} to 5.10^{-3} m (Gualtieri and Secci 2011), we applied a rough wall condition for BC3 with $y_0 = 3.10^{-3}$ m (Manwell *et al.* 2009). It is well known that the wake development is influenced by the local topography and roughness, especially when the hub height is embedded in the Atmospheric Boundary Layer. Others values are applied for sandy, rocky, dense forest, or for offshore cases (Paskyabi 2015). Different laws are also suggested to compute y_0 (Stull 1988). These cases are not considered in this study.

The applied boundary conditions are summarized in Table 1.

Table 1 Computational domain boundary conditions.

Boundary	Conditions
BC1	Velocity inlet
BC2	symmetry
BC3	Wall
BC4	symmetry
BC5	symmetry
BC6	pressure outlet

6.4 Algorithm and Schemes

The SIMPLE algorithm is used for the pressure-velocity coupling. The second order upwind and first order upwind schemes are applied for the momentum and turbulence equations respectively.

The time step is set to $\Delta t = 0.0001$s, giving a CFL number of about 1 to ensure the flow stability (Blocken *et al.* 2010). Calculations were run for more than 4000 time steps, which correspond to the physical time t=0.4 s and about 80 revolutions of the rotor. Thereby, wake stability is ensured and sufficient informations about the wake flow structures are obtained. The convergence criterion was set to 10^{-6} for the residuals of the continuity equation.

6.5 Grid sensitivity

A mesh sensitivity test is conducted to improve the quality of the computational results and to optimize the simulation cost and accuracy as in numerous works among which (Hussein and El-Shishiny 2012; Alinot and Masson 2005; Réthore *et al.* 2014). These later compared the number of nodes per rotor diameter required to capture the wake turbulence. They assessed 4, 8, 16 and 32 nodes/rotor diameter and demonstrated that 8 cells per rotor diameter are sufficient and are recommended in the wake study. Their resulting relative error was less than 1%, however they concluded that the mesh study should take into account the CPU computation time.

In this work, four grids were tested, coarse, thin and medium, the number of cells is increased in a homogeneous way in the three flow directions so as not to disturb the topology of the domain (Van der Laan *et al.* 2015). The absolute relative error ε (%), between the rotor average axial velocity and the experimental data is calculated at the hub height level using the following relation:

$$\epsilon = \frac{u_{\exp} - \overline{u}}{u_{\exp}} \qquad (25)$$

The error is calculated for two distances downstream of the rotor, z=5D and z=7D. The obtained results obtained are summarized in Table 2 which shows that the relative errors obtained with meshes 3 and 4 are equal to 3% at z=5D and 5.9% for z=7D. These results indicate that mesh 3 is well suited for this study.

Table 2 Grid sensitivity analysis.

Grid level	Cell number	abs relative error (%) z/D=5	abs relative error (%) z/D=7
1	966527	19.2%	5.8%
2	1933054	19.1%	5.6%
3	3 866 109	3%	5.6%
4	4627959	3%	5.6%

7. RESULTS AND DISCUSSIONS

The wake expansions of the wind turbine are investigated for two hub height to diameter ratios, h/D = 0.7 and h/D= 1, in order to estimate the ground influence.

The measured data are described by the average axial velocity and the vorticity expressed in a dimensionless form by the following equations:

$$\overline{U} = \frac{U(z)}{U_0} \qquad (26)$$

$$\overline{\Omega} = \frac{\omega_z D}{U_0} \qquad (27)$$

The average velocity field is reconstituted from correlations used to calculate the displacements of the particles on all the recording planes. This averaging permits a better reveal of the wake/wall interaction averaged snapshots. Data from a velocity field around the tip vortices using this technique are of high quality.

The measured and computed average axial velocity contours are depicted in Figs. 8 and 9 for h/D = 0.7 and h/D = 1, respectively.

The experimental velocity contours represented in Figs. 8a and 9a, are the average data of all measurement planes. These figures show the wake progression in the direction (z), from a distance of 1D up to 7D downward the rotor. Figures 8-b and 9-b represent the numerical results.

On the whole, the numerical results are in good agreement with the experimental data. Indeed, both results show that the domain lower half (close to the ground), is immersed within the developed boundary layer (at h/D=0.7) differing from the second case study (h/D=1), which is outside the boundary layer as close as neighborhood. Also, for both h/D ratios, the wall has a significant impact on wake development. Due to the wall/wake interaction, the wake expansion is damped and is parallel to the wall and has a width of 1 D.

For h/D = 0.7, Figs. 8a and 8b show a confined flow which forms a boundary layer around the blade and generates swirling vortex which break off along the blade. Flow detachment occurs downstream the rotor. In addition, the swirling vortices escape from the root faster, as the speed decreases and the drag force effect increases at this level. The experimental results show that the vortices appear first in the form of small isolated vortex structures at a distance less than z=0.5D (Fig. 8a). Whereas for the numerical results, the formation of these vortex structures becomes visible at z = 1D, then the vortices merge to form a continuous sheet, which extends up to z=2D (Fig. 8b). This continuous sheet formation is also observed on Fig. 8a.

From the first cycles of revolution, a significant drop in the axial velocity is recorded at the center of the wake, caused by the disintegration of the vortices generated by the blade tips (Fig. 8b). This low speed zone defines the near wake region which extends up to z=3D (Dobrev *et al*. 2008). At ground level, the flow generated by the blade is slowed down, inducing low flow velocities. As noticed by (Kamada and Maeda 2011), the appearance of the lower vortices is delayed compared to the upper vortices (Fig. 8a). This braking is distorted at a distance of z=2D downstream and disappears at z=4D.

Both Figs. 8a and 8b show that in the near wake region, the flow velocity increases at the ends of the rotor, due to the separation of the accelerated fluid particles of the blade tips. The gradual detachments of these vortices help to create a separation layer between the wake and the developed flow zone.
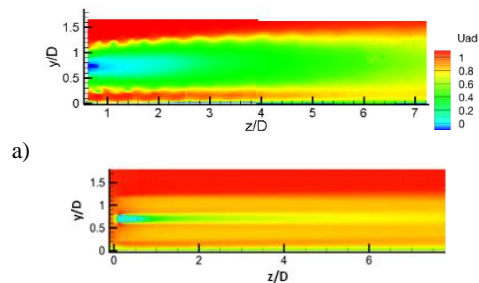

Fig. 8. Contours of the axial velocity for *h/D*=0.7 in the zy plane. a) Experimental data. b) Numerical results.

For the case h/D =1 (Fig. 9a & 9b), the results show that the rotor operates outside the wall boundary layer, however, the influence of the latter is visible.

Both figures show that the vortices appearance remains insensitive to the wall effect. However, Fig. 9a, show that the axis of the wake is deflected upward. Two vortices are formed and propagate at low speed until they come together and form a single vortex (Fig. 9a). These experimental outcomes are not seen in the numerical results of Fig. 9b.

The flow is slower in the lower area of the wind tunnel, near the ground. The attenuation of the vortex structures begins at a distance z=4D (Fig. 9a, 9b). Indeed, at the distance z = 5D corresponding to the end of the near wake zone, there is a transition zone towards the far wake, from which the effects of aerodynamic turbulence are gradually dissipated from z> 7D.

The small tip vortices, involving the near wake downstream of the rotor and delimiting the wake area on both sides, are more perceptible in the experimental results (Fig. 9a). This is probably due to the AD numerical model that does not allow a detailed description of the flow in the vicinity of the rotor at distances lower than 1D. However, the simulation results provide good information on wake behavior beyond 1D. These results confirm that the AD model gives a good representation of the wake behavior downstream, but does not reproduce blade tip vortices near the rotor. This was also observed by (Porté-Agel *et al.* 2011; Daaou Nedjari *et al.* 2020; Alinot and Masson 2005), whom suggested the use of the actuator line model to reproduce the eddy tip vortex, for which a fine description and more detailed grid are needed. In this study, the applied correction model of the blade tip losses considers the fraction of the kinetic energy transmitted to the blade tip vortex. Therefore, the downstream flow structures provided by the AD model are sufficiently representative. Thereby, typical characteristics of the wind turbine wake are reproduced such as the increase in the level of turbulent kinetic energy, the formation of the deficit zone and the scattering of the wake in the ground boundary layer, illustrated by Figs. 8b and 9b.
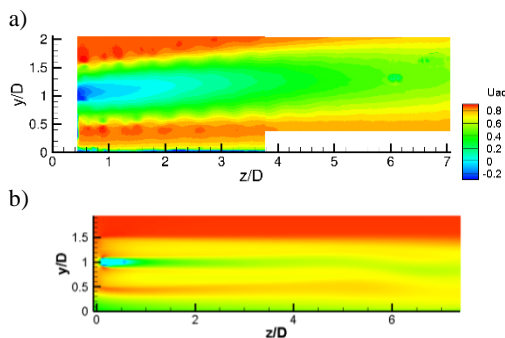

Fig. 9. Contours of the axial velocity for *h/D*=1 in the zy plane. a)- Experimental data. b)- Numerical results.

The vorticity contours are represented in Figs. 10 and 11 for the two hub heights h/ D = 0.7 and h/D =1. These figures show that the wake is characterized by helical swirling vortices, which are distinctly created from the downstream flow with velocity deficits that

vary along the axis of rotation and that are driven by the downstream flow constituting the near wake.

The flow becomes diffusive and small turbulent structures disappear under the influence of the turbulence. The swirling vortices generate the far wake beyond z = 6 D.

The vortex structures are clearly observed in the vorticity field depicted in Figs 10 and 11. Counter-rotating vortex structures generated by the detachment of the vortices from the surface of the blade are observed. The appearance of these vortices is due to the existence of a circulation discontinuity along the blade as confirmed experimentally by (Kamada and Maeda 2011). The later reported that at low TSR, this results in the creation of two adjacent counter-rotating vortices, where the blade root section has a high angle of attack.
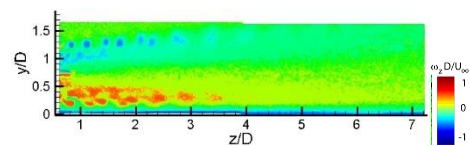

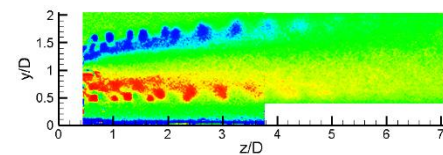**Fig. 10. Experimental results of vorticity contours in the zy plane for *h/D*=0,7.**

Fig. 11. Experimental results of Vorticity contours in the zy plane for *h/D*=1,0.

The profiles of the vertical velocity, which correspond to the wind speed deficit downstream the rotor, are analyzed and compared to the experimental measurements. These comparisons, depicted in Figs. 12 and 13, are performed for axial positions varying from z /D = 1 to z/D=7

The shape of the curves shows that the wake has a thickness of 1D and is not symmetric. This is due to the non-uniformity of the inlet velocity profile as well as to the shear stress created in the ground vicinity. Initially, a velocity deficit of 20% in the wake axis is obtained at z= 1D; the velocity deficit increases progressively up to 70% at z= 7D. It is clearly seen that the wake adheres to the ground boundary layer for h/D = 0.7 (Fig. 12). The interaction effect is lower for h/ D = 1.0 (Fig. 13), where the wake centerline is shifted by about 0.3D upward. At 1D downstream, the flow, outside the wake, accelerates due to the tip vortices presence, which are clearly observed in the wake upper part. A difference between the experimental and the numerical values is observed in the near wake region (at z/D=1 and 2). These differences are attributed to the additional effects of the centrifugal and Coriolis forces (Zhaohui 1997) that are neglected in the 2D drag and lift coefficients used in this study. For z≥3 D, the numerical results are in good agreement with the experimental data.
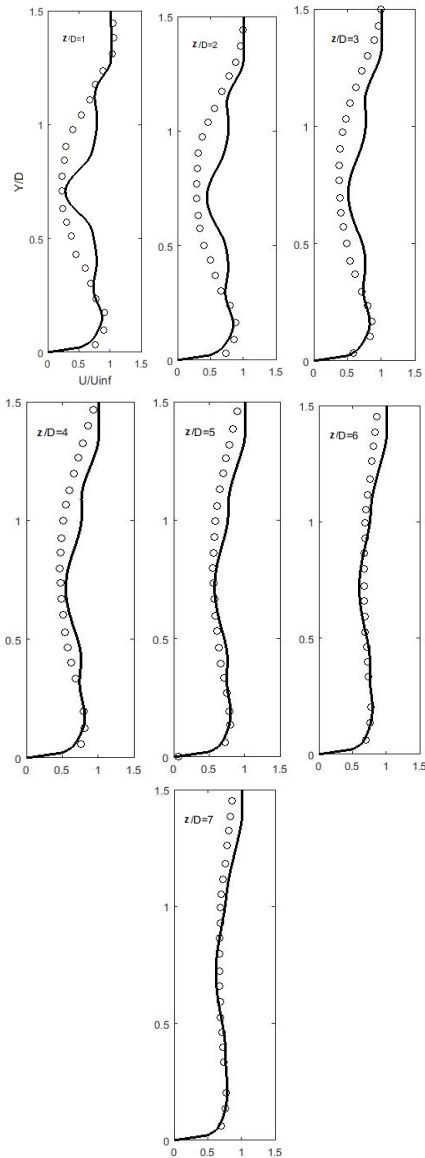
show the effect of the tangential force intensity on the wake structure at each position downstream the rotor.

Fig. 12. Axial velocity profile at z/D = 1 to 7, for *h/D* = 0.7. - Experimental data (o). - Simulation results (—).

Figure 14 shows the evolution of the turbulent kinetic energy in the lateral (a) and the radial (b) directions. A significant release of turbulent energy K occurs along the rotor, with the appearance of a peak at the center (Fig. 14a). In the radial direction, the turbulent kinetic energy K increases in the center of the rotor along the z direction (Fig. 14b). K is more important in the near wake due to the diffusion and decreases in the far wake. The swirling vortices appear at the tip of the blade at about r/R = 0.5. These structures, produced by the blade's movement, dissipate gradually downstream the rotor. However, the turbulent energy does not decrease such as the atmospheric turbulence; Moreover, shear layers are present in the flow and maintain the turbulence in the far wake.

Figures 15 and 16, represent the streamlines in six cross section planes varying from z = 3D to z=10D, for h/D = 0.7 and h/D=1 respectively. These figures
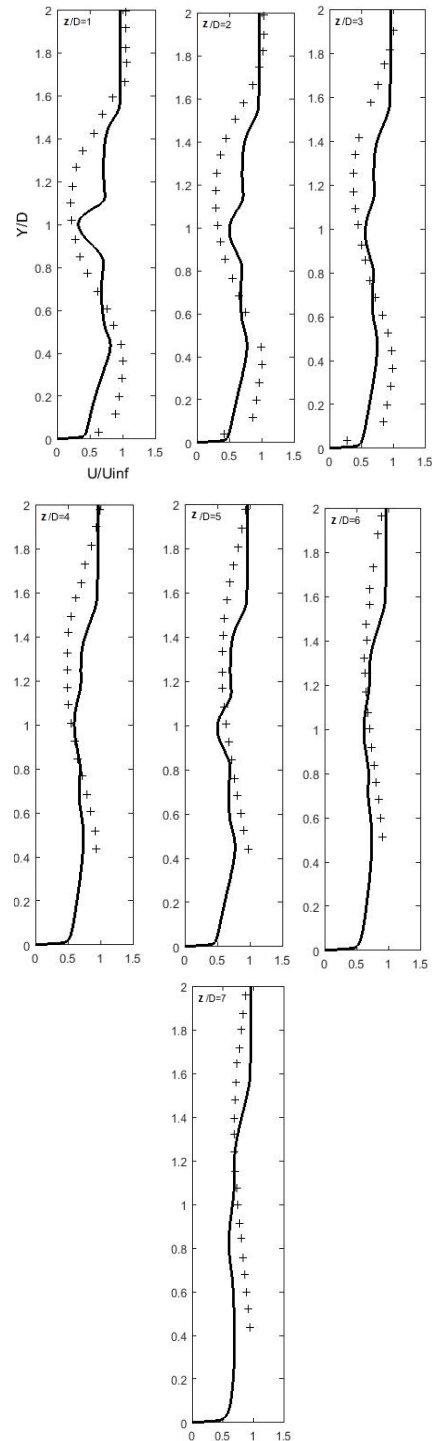

Fig. 13. Axial velocity profile at z/D = 1 to 7, for *h/D*=1. - Experimental data (+). - Simulation results (—).

As observed in the velocity contours (Figs. 8 and 9), the streamlines are not symmetrical according to the axis of rotation. This is due to the inlet velocity profile and the ground boundary layer. The effect of
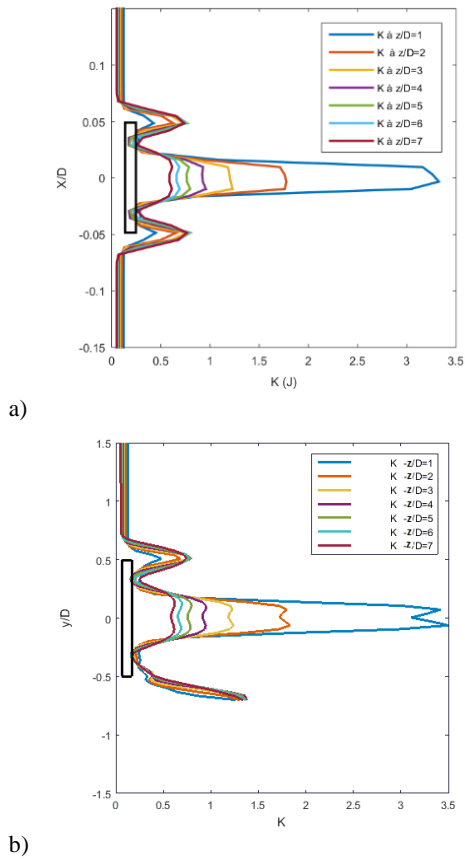
a)

b)

Fig. 14. Turbulent kinetic energy variation at different axial positions for h/D=0,7. a) - In the lateral direction. b) - In the radial direction.

the rotation persists up to 7D downstream of the rotor, this is shown in the far wake extent, and

disturbs the downstream flow beyond 10D as noticed by Wu and Porté-Agel (2011).

Figures 15 show that the wind turbine wake interacts strongly with the ground when h/D=0.7. Indeed, for the nearest distance to the ground, h/D=0.7 (Fig. 15), it can be seen that the wake of the wind turbine is disturbed by the shear phenomenon created by the ground boundary layer. Figures 15-d, 15e and 15-f show that at the distance z= 6D (Fig. 15d) up to z=10D (Fig.15f), a vortex forms near the floor of the wind tunnel. This vortex roll, approximately 4D in length, develops along the longitudinal direction, in the lower part of the wake, more precisely in the shear zone close to the ground, at less than y=0.5D. This interaction of the ground with the vortex zone induces an attraction of the wake center downwards resulting in an asymmetrical wake. This phenomenon was also shown by Espana (2009).

For the case h/D=1, Figure 16 shows that the interaction between the wind turbine wake and the ground is less important. The rotation of the wake streamlines at z=3D is clearly independent of the ground and the wake zone is more axisymmetric. At distances z=4D and z=5D (Figs.16b and 16c), the streamlines close to the ground are slightly deformed but the wake zone remains well defined. At z=6D (Fig. 16d), we observe a streamline expansion that represents the beginning of the wake dissipation. This is the transition zone to the far wake. The effects of aerodynamic turbulence dissipate gradually when z > 7D (Fig. 16e) where the overlap reaches 70% and dissipate almost completely at z=10D (Fig. 16f). On the other hand, for the case h/D =0.7, the expansion of the streamlines in the wake is not observed even at the distance z = 10D (Fig. 15f). The wake dissipation, therefore occurs more quickly in the case h/D=1 compared to the case h=0.7D.
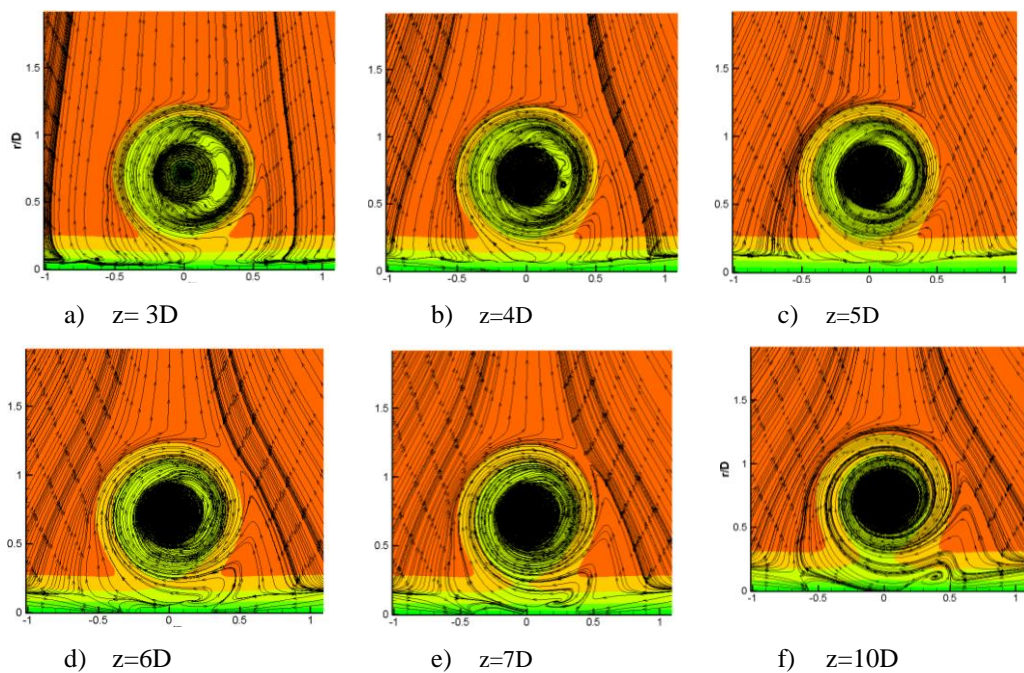

a)   z= 3D

b)   z=4D

c)   z=5D

d)   z=6D

e)   z=7D

f)   z=10D

Fig. 15. Streamlines in the xy planes at different axial positions for h/D=0.7 case.
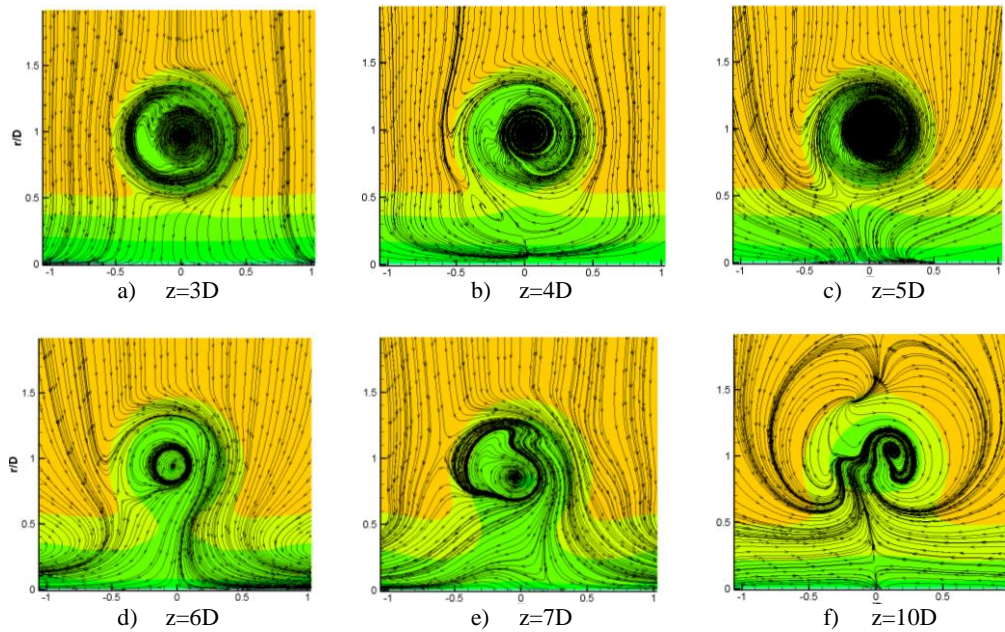
Fig. 16. Streamlines in the xy planes for h/D=1.

8. Conclusion

This paper described numerical and experimental investigations of the hub height effects on the near and far wake of a two bladed horizontal axis wind turbine.

For the numerical study, a hybrid BEM-Actuator Disk was used. In the experimental study, the flow velocity was explored using Particle Image Velocimetry (PIV). These measurements allowed to highlight a set of phenomena that were obtained by the numerical simulations.

The results obtained show that the wake is triggered by an important mechanism of vortices, which originate at the blades top of the rotor. A composition of bubbles appears near the hub causing a recirculation zone thus breaking the turbulence. The wake appears gradually in the axial direction downstream of the rotor. The vortex system composed of tip vortices starts to appear at a distance of 2.5 D downstream. The diffusion occurs gradually until it settles at 4D downstream.

At h/D =0.7 the rotor operates in the boundary layer. The tip vortices developed in the lower part are slower than those in the upper half, their development take place mainly in the horizontal direction. It is observed that the wake develops beyond the boundary layer and the tip vortices is progressing, on each side of the wake, at the same time for the ratio h/D=1, The main observation is that the ground effect is present in both cases. It was observed that the wake centerline is upward deflected at about 0.3D for the case h/D = 1. It is concluded that the hub height be required above 1D to limit the influence of the ground boundary layer effect.

Both numerical results and experimental data, showed a gradual velocity deficit for distances varying from 1D to 7D. A lag was noted between the vertical profiles of the experimental and numerical wind velocity in the near wake (at z=1D). This mismatch is attributed to the data used for C_L and C_D coefficients that do not consider the centrifugal and Coriolis forces.

This study highlighted the detailed structure of the wake and the hub height effects of a horizontal axis wind turbine. The identification of vortex structures that are diffused in the far wake, are useful to determine the distance that must be observed between wind turbines and to optimize the wind farm performance. As a continuity of this work, the study of the rotation effect is in progress in order to improve the results of the applied model.

These results show that the effects of the ground on the wake development are significant when the mast height is less than 1D. These ground-wake interactions must be taken into account when optimizing the location of wind turbines in a wind farm.

REFERENCES

Abdulrahim, A., A. Ezgi, O. Yashar and U. Oguz (2016). Effects of tip injection on the performance and near wake characteristics of a model wind turbine rotor. *Renewable Energy* 88, 73-82.

Abkar, M. and F. Port´e-Agel (2014). The effect of atmospheric stability on wind-turbine wakes: A large-eddy simulation study. *Journal of Physics: Conference Series* 524 012138.

Alinot, C. and C. Masson (2005). k-ε Model for the Atmospheric Boundary Layer under Various Thermal Stratifications. Journal of Solar Energy Engineering 127(November).

Ammara, I., C. Leclerc and C. Masson (2002). A viscous three-dimensional method for the aerodynamic analysis of wind farms. Journal of Solar Energy Engineering 124, 345–356.

Aubrun, S., S. Loyer, P. E. Hancock and P. Hayden (2013). Wind turbine wake properties: Comparison between a non-rotating simplified wind turbine model and a rotating model. *Journal of Wind Engineering and Industrial Aerodynamics* 120 1–8.

Blocken, B., G. Dezsö, J. van Beeck and J. Carmeliet (2010). Comparison of calculation models for wind-driven rainde position on building facades. *Atmospheric Environment* 44 (14), 1714–1725.

Blocken, B., J. Carmelieta and T. Stathopoulos (2007). CFD evaluation of wind speed conditions in passages between parallel buildings—effect of wall-function roughness modifications for the atmospheric boundary layer flow. *Journal of Wind Engineering and Industrial Aerodynamics* 95 941–962.

Boojari, M., E. Mahmoodi and A. Khanjari (2019). Wake modelling via actuator-line method for exergy analysis in openFOAM, *International Journal of Green Energy* 16(11), 797-810.

Breton, S. P. (2008). A Study on Different Stall Delay Models Using a Prescribed Wake Vortex Scheme and NREL Phase VI Experiment. *Wind Energy* 11, 459–482.

Chamorro, L. P, M. Guala, R. E. A. Arndt and F. Sotiropoulos (2012). On the evolution of turbulent scales in the wake of a wind turbine model, *Journal of Turbulence* 13, N27.

Cillis, G., S. Cherubini, O. Semeraro, S. Leonardi and P. De Palma1 (2021). Pod‑based analysis of a wind turbine wake under the influence of tower and nacelle. *Wind Energy* 24, 609-633.

Daaou Nedjari, H., O. Guerri and M. Saighi (2017). CFD wind turbines wake assessment in complex topography. *Energy Conversion and Management* 138, 224–236.

Daaou Nedjari, H., O. Guerri and M. Saighi (2020). Full rotor modelling and generalized actuator disk for wind turbine wake investigation. *Energy Reports* 6, 232-255.

Dobrev, I. (2009). Active surface hybrid model for the analysis of the aerodynamic behavior of wind turbine rotors with rigid or deformable blades. Ph. D. thesis, Arts et Métiers ParisTech, France.

Dobrev, I., B. Maalouf, N. Troldborg and F. Massouh (2008). Investigation of the wind turbine vortex structure. *14th Int Symp on Appl of Laser Tech to Fluid Mech*, Lisbon Portugal, 1-7.

Dobrev, I., F. Massouh and A. Memon (2013). Experimental and numerical study of flow around a wind turbine rotor. *International Journal of Engineering Systems Modelling and Simulation* 5(1), 137-146.

Dobrev, I., F. Massouh and M. Rapin (2007). Actuator surface hybrid model, *Journal of Physics: Conference Series* 75(1), 012019.

Ducoin, A., M. S. Shadloo and S. Roy (2017). Direct Numerical Simulation of flow instabilities over Savonius style wind turbine blades. *Renewable Energy* 105, 374-385.

El Kasmi, A. and C. Masson (2008). An extended k-ε model for turbulent flow through horizontal-axis wind turbines. *Journal of Wind Engineering and Industrial Aerodynamics* 96, 103–122.

El-Askary, W. A., I. M. Sakr, M. Ali, M. R. AbdelSalam and M. Abuhegazy (2017, January). Modeling of wind turbine wakes under thermally-stratified atmospheric boundary layer. *Journal of Wind Engineering and Industrial Aerodynamics*160, 1-15.

Espanâ, G. (2009). *Experimental Study of the Long Wake of Horizontal Axis Wind Turbines Using Simplified Atmospheric Boundary Layer Modeling.* Ph.D. thesis, Université d'Orléans, Orléans, France.

Espanâ, G., S. Aubrun, S. Loyer and P. Devinant (2012). Wind tunnel study of the wake meandering downstream of a modelled wind turbine as an effect of large scale turbulent eddies. *Journal of Wind Engineering and Industrial Aerodynamics* 101, 24–33.

Gao, Z., Y. Li, T. Wang, S. Ke and D. Li (2021a). Recent improvement of actuator line model in the large-eddy simulation of wind-turbine wakes. *Applied Mathematics and Mechanics* 42, 511-526.

Gao, Z., Y. Li, T. Wang, W. Shen, X. Zheng and S. Pröbsting（2021b）. Modeling the nacelle wake of a horizontal-axis wind turbine under different yaw conditions. *Renewable Energy* 172263-275.

García Regodeseves, P. and C. Santolaria Morros (2021). Numerical study on the aerodynamics of an experimental wind turbine: Influence of nacelle and tower on the blades and near-wake. *Energy Conversion and Management* 237, 114110.

Gualtieri, G. and S. Secci (2011). Wind shear coefficients, roughness length and energy yield over coastal locations in Southern Italy. *Renewable Energy* 36 1081-1094.

Gunn, K. (2019). Improvements to the Eddy Viscosity Wind Turbine Wake Model. *IOP Conf. Series: Journal of Physics:* Conf. Series 122, 2012003,

Hong, J. (2014). Natural snowfall reveals large-scale flow structures in the wake of a 2.5 MW wind turbine. *Nature Communications* 5, 4216.

Hussein, A. S. and H. E. El-Shishiny (2012).

Modeling and simulation of micro-scale wind farms using high performance computing. International Journal of Computational Methods 9(2) 1240025.

Javaherchi, T., S. Antheaume and A. Aliseda (2014). Hierarchical Methodology for the Numerical Simulation of the low Field around and in the Wake of Horizontal Axis Wind Turbines: Rotating Reference Frame, Blade Element Method and Actuator Disk Model. *Wind Engineering* 38(2) 181-202.

Johlas, H. M., D. P. Schmidt and M. A. Lackner (2022). Large eddy simulations of curled wakes from tilted wind turbines. *Renewable Energy* 188349-360.

Kamada, Y. and T. Maeda (2011). Experimental studies on velocity field around wind turbine rotor. *International Conferance and Utility Exhibition on Power and Energy Systems (ICUE) IEEE* 2011, 1-7.

Makridis, A. and J. Chick (2013). Validation of a CFD model of wind turbine wakes with terrain effects. *Journal of Wind Engineering and Industrial Aerodynamics* 123, 12–29.

Manwell, J. F., J. G. McGowan and A. L. Rogers (2009). *Wind Energy Explained*, second ed. Wiley.

Masson, C. (2006). Numerical Study of Turbulent Flow around a Wind Turbine Nacelle. *Wind Energy* 9, 281–298.

Massouh, F. and I. Dobrev (2007). Exploration of the vortex wake behind of wind turbine rotor. *Journal of Physics: Conference Series* 75 012036.

Orlandi, P. and S. Leonardi (2006). DNS of turbulent channel flows with two- and three-dimensional roughness, *Journal of Turbulence* 7, N73.

Panofsky, H. A. and J. A. Dutton (1984). *Atmospheric Turbulence.* John Wiley & Sons, New York, U.S.A.

Panofsky, H. A. (1988). The effect of averaging time on velocity variances. *Meteorology and Atmospheric Physics* 38, 64–69.

Paskyabi, M. B. (2015). Offshore Wind Farm Wake Effect on Stratification and Coastal Upwelling. *Energy Procedia* 80, 131 – 140.

Porté-Agel, F. (2011). Large-eddy simulation of atmospheric boundary layer flow through wind turbines and wind farms. *Journal of Wind Engineering and Industrial Aerodynamics* 99, 154–168.

Porté-Agel, F., M. Bastankhah and S. Shamsoddin (2020). Wind-Turbine and Wind-Farm Flows: A Review. *Boundary-Layer Meteorology* 174, 1–59.

Réthoré, P. E., P. van der Laan, N. Troldborg, F. Zahle and N. N. Sørensen (2014). Verification and validation of an actuator disk model. *Wind Energy* 17, 919–937.

Shen, W. Z, R. Mikkelsen, J. Nørkær Sørensen and C. Bak. (2005). Tip loss corrections for wind turbine computations.

Shen, W., J. Zhang and J. Sørensen (2009). The actuator surface model: a new Navier–Stokes based model for rotor computations. *Journal of Solar Energy Engineering* 131(1), 011002.

Simisiroglou, N., S. Sarmast, S. P. Breton and S. Ivanell (2016). Journal of Physics Conference Series 753 032028.

Sørensen, J. and A. Myken (1992). Unsteady actuator disk model for horizontal axis wind turbines. *Journal of Wind Engineering and Industrial Aerodynamics* 39(1), 139-149.

Stevens, R. J. A. M., L. A. Martínez-Tossas and C. Meneveau (2017). Comparison of wind farm large eddy simulations using actuator disk and actuator line models with wind tunnel experiments, *Renewable Energy* 116(A), 470-478.

Stull, R. B. (1988). *An Introduction to Boundary Layer Meteorology.* ISBN: 978-94-009-3027-8.

Tominaga, Y., M. Akashi, Y. Ryuichiro, K. Hiroto, N. Tsuyoshi and Y. Masaru (2008, October–November). AIJ guidelines for practical applications of CFD to pedestrian wind environment around buildings. *Journal of Wind Engineering and Industrial Aerodynamics* 96(10–11), 1749-1761.

Van der Laan, P., M., N. Niels, Sørensen, P. E. Réthoré, J. Mann, Mark C. Kelly, N. Troldborg, J. G. Schepers and E. Machefaux (2015). An improved k-ε model applied to a wind turbine wake in atmospheric turbulence. *Wind Energ* 18, 889–907.

Vermeer, L. J. (2003). Wind turbine wake aerodynamics. *Progress in Aerospace Sciences* 39. 467–510.

Wind energy in Europe in 2019 Repport (2019). (https://windeurope.org/).

Wu, Y. T. and F. Porté-Agel (2011). Large-Eddy Simulation of Wind-Turbine Wakes: Evaluation of Turbine Parametrisations. *Boundary-Layer Meteorol* 138, 345–366.

Zhaohui, D. (1997). *A 3-D Stall-Delay Model for Horizontal Axis wind Turbine Performance Prediction.* American Institute of Aeronautics and Astronautics, Inc.